Supporting Information

Structural regulation of ionic covalent organic frameworks for enhanced CO_2 capture and catalytic conversion

Xiaoqing Yang,[a] Bihua Chen,[a,b] Junfeng Zeng,[a] Zhiyong Li,[c] Yan Zhang[a,*] and Shiguo Zhang[a]

[a]College of Materials Science and Engineering, Hunan University, Changsha 410082, Hunan, China

[b]Key Laboratory of Materials Physics, Centre for Environmental and Energy Nanomaterials, Anhui Key Laboratory of Nanomaterials and Nanotechnology, Institute of Solid State Physics, HFIPS, Chinese Academy of Sciences, Hefei 230031, Anhui, China

[c]School of Chemistry and Chemical Engineering, Henan Normal University, Xinxiang 453007, Henan, China

E-mail: zyan1980@hnu.edu.cn

1. Gram-scale synthesis of NKCOF41 and various ionic COFs

1.1. Synthesis of NKCOF41

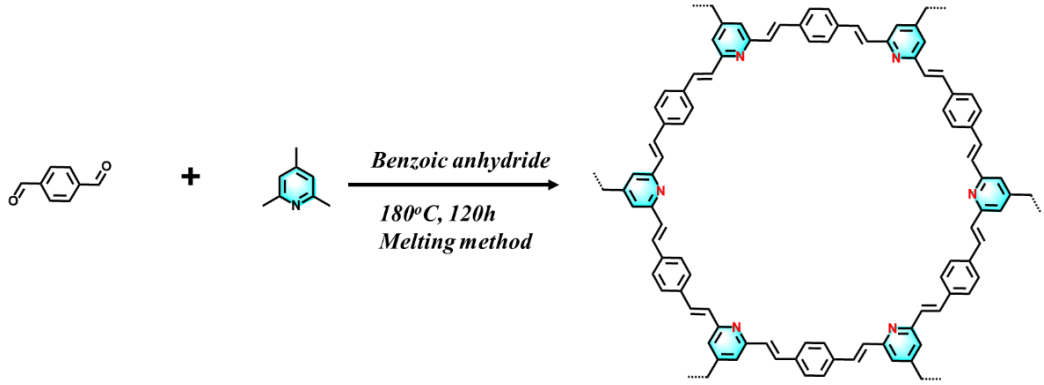

Scheme S1 Schematic diagram of NKCOF41 synthesis.

First, as shown in **Scheme 1**, using 2,4,6-trimethylpyridine (TMP, 1225 μL, 10 mmol) and terephthalaldehyde (TPA, 2010 mg, 15 mmol) as the reaction monomers, and selecting benzoic anhydride (BA, 2255 mg, 10 mmol) as the melting agent, a large quantity of microporous pyridine-based COF material (NKCOF41) with high specific surface area was successfully synthesized (90% yield).

1.2. Synthesis of NKCOF41^{+}–$C_2H_4OHBr^{-}$

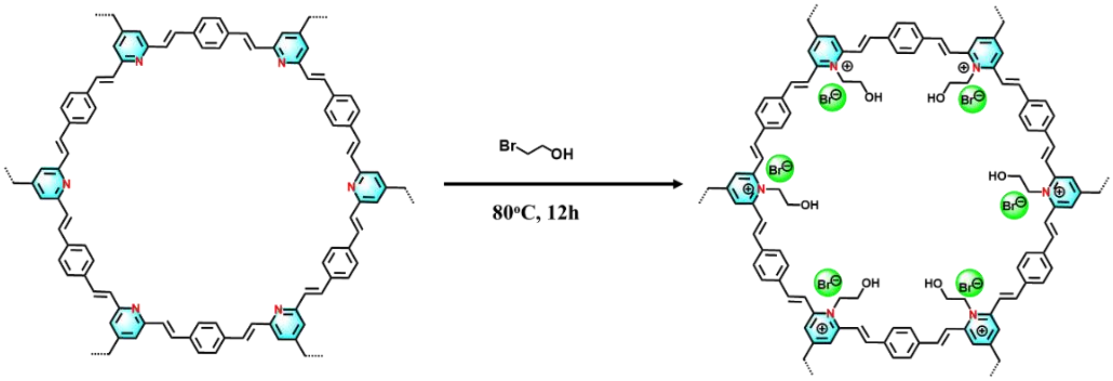

Scheme S2 Schematic diagram of NKCOF41^{+}–$C_2H_4OHBr^{-}$ synthesis.

1.3. Synthesis of NKCOF41H^{+}–Br^{-}

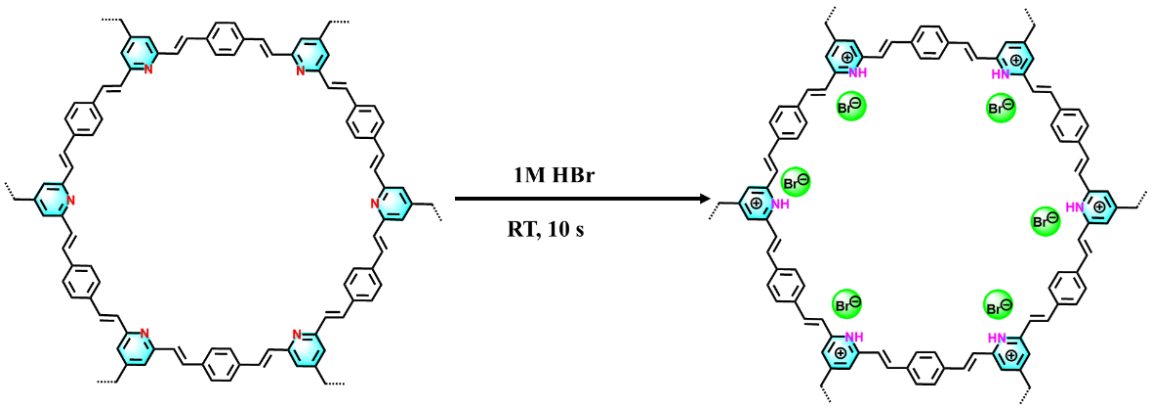

Scheme S3 Schematic diagram of NKCOF41H^{+}–Br^{-} synthesis.

As shown in Scheme S3, NKCOF41 (1.00 g) was directly dispersed in 20 mL of 1 M hydrobromic acid (HBr) (0.02 mol, 1.62 g), ultrasonicated for 10 s, and the solid product was collected by centrifugation. It was purified via Soxhlet extraction with deionized water and ethanol (24 h each), and then vacuum-dried at 100 °C for 12 h to obtain 1.16 g of the protonated functionalized product NKCOF41H^{+}–Br^{-} (92% yield).

1.4. Synthesis of NKCOF41^{+}-$C_2H_5Br^{-}$

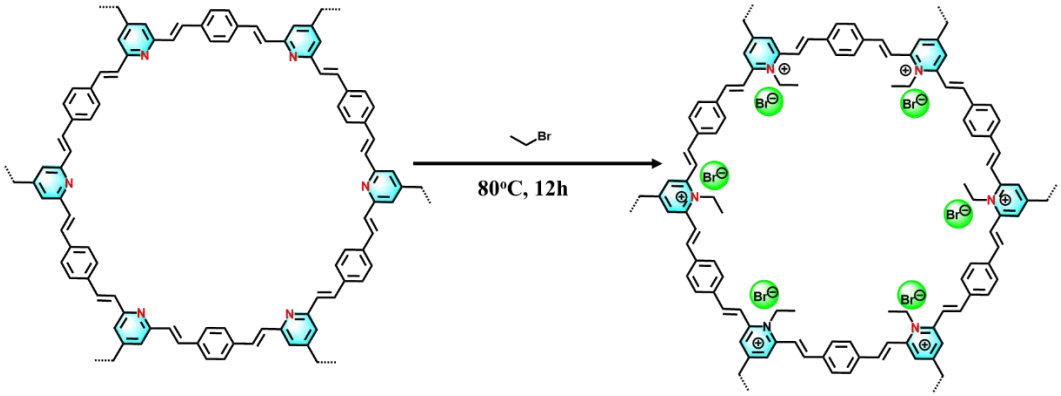

Scheme S4 Schematic diagram of NKCOF41^{+}–$C_2H_5Br^{-}$ synthesis.

As shown in **Scheme S4**, NKCOF41 (1.00 g) was dispersed in anhydrous ethanol (20 mL), and excess bromoethane (0.05 mol, 5.45 g) was added under reflux for 24 h. The solid product was collected by centrifugation, purified via Soxhlet extraction with ethanol (24 h), and dried under vacuum at 100°C for 12 h to afford 1.2 g of the ionic covalent organic framework (denoted as NKCOF41^{+}–$C_2H_5Br^{-}$) in 85% yield.

2. Adsorption Isotherm Analysis

Adsorption Isotherm Analysis

To elucidate the adsorption thermodynamics and surface interactions, two classical isotherm models – Langmuir and Freundlich – were applied to interpret the equilibrium data.

Langmuir Isotherm Model: This model postulates monolayer adsorption on homogeneous surfaces with energetically equivalent sites. The separation factor (RL = $[1/(1+b\times P_e)]$, ranging between 0.47 and 0.98 across all systems, confirmed favorable adsorption conditions ($0 < RL < 1$). The nonlinearized Langmuir equation is expressed as:

$$q = \frac{Q_o b P_e}{1+bP_e} \quad (1)$$

where Q_0 denotes theoretical monolayer capacity (derived from slope analysis), b represents the affinity constant (calculated from intercept), and P_e is equilibrium pressure.

Freundlich Isotherm Model: As an empirical model describing heterogeneous adsorption systems, the Freundlich equation effectively characterizes multilayer sorption processes. All derived exponent values ($n > 1$) suggest favorable CO_2 uptake on COF, through combined physicochemical interactions. The mathematical expression is given by:

$$q = K_f (P_e)^{\frac{1}{n}} \quad (2)$$

where K_f reflects adsorption capacity (determined from intercept) and the dimensionless

parameter n (obtained from slope) quantifies adsorption intensity and surface heterogeneity.

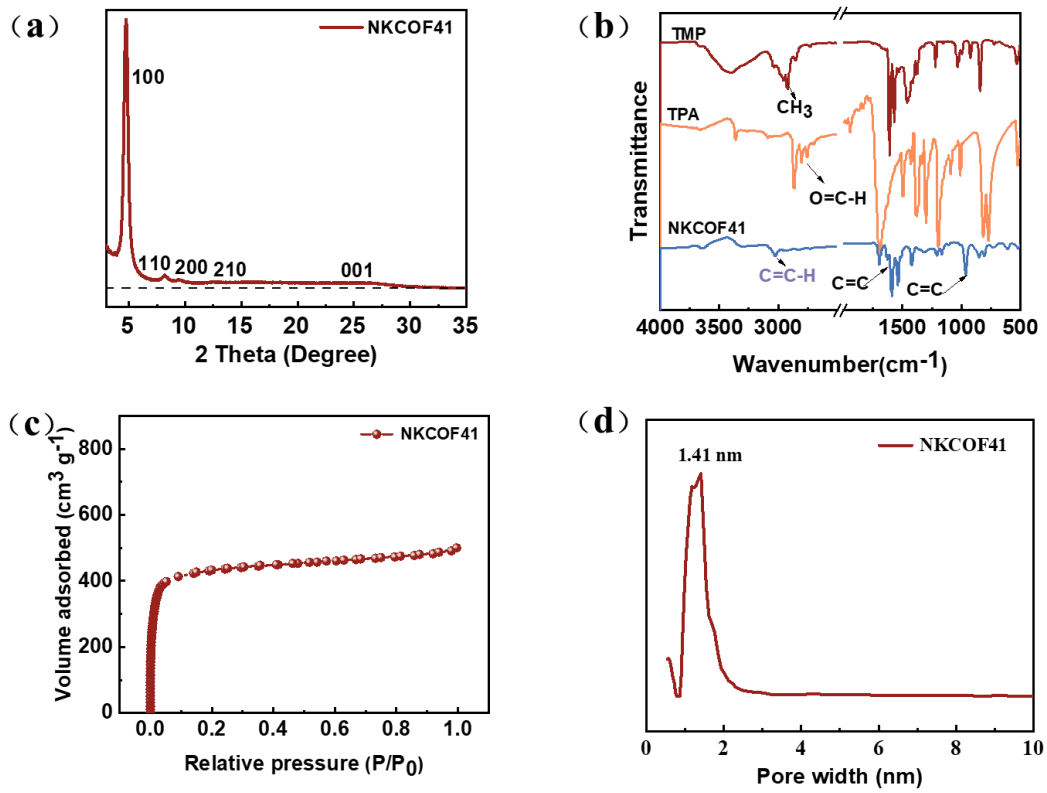

Fig. S1 (a) PXRD pattern of NKCOF41; (b) FT-IR spectra of TMP, TPA, and NKCOF41; (c) N_2 adsorption-desorption isotherm of NKCOF41 at 77 K; (d) NKCOF41 pore distribution calculated by quenched solid density functional theory.

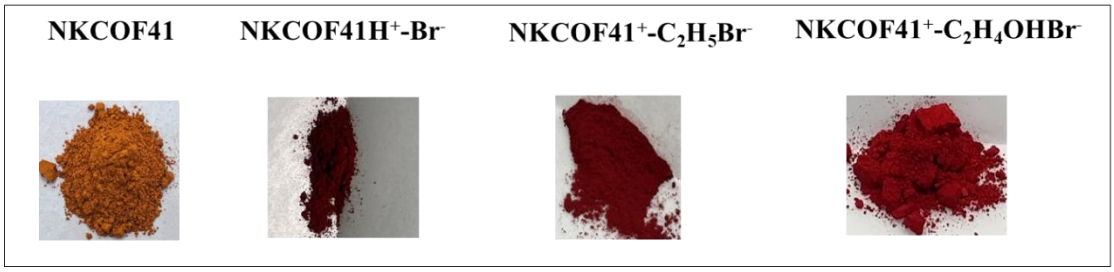

Fig. S2 NKCOF41 and ionic COF powders.

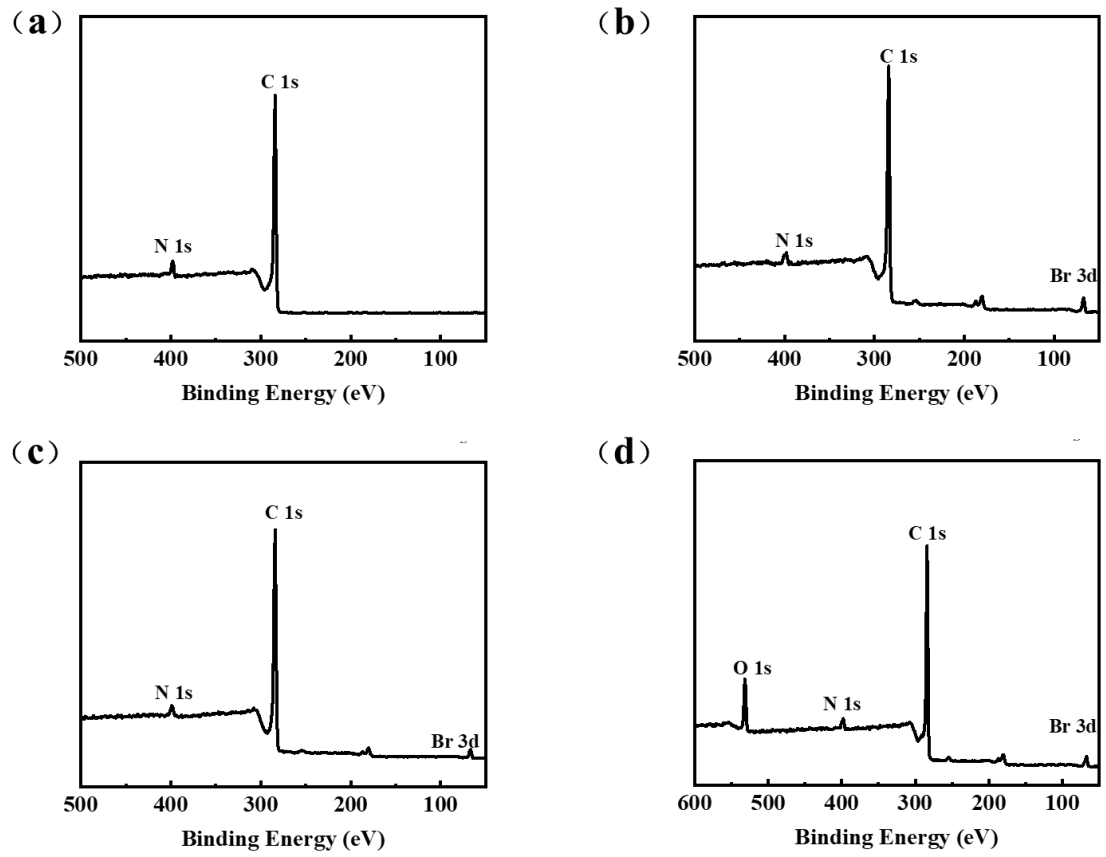

Fig. S3 XPS spectra of NKCOF41 (a), NKCOF41H^+–Br^- (b), NKCOF41$^+$–$C_2H_5Br^-$ (c), and NKCOF41$^+$–$C_2H_4OHBr^-$ (d).

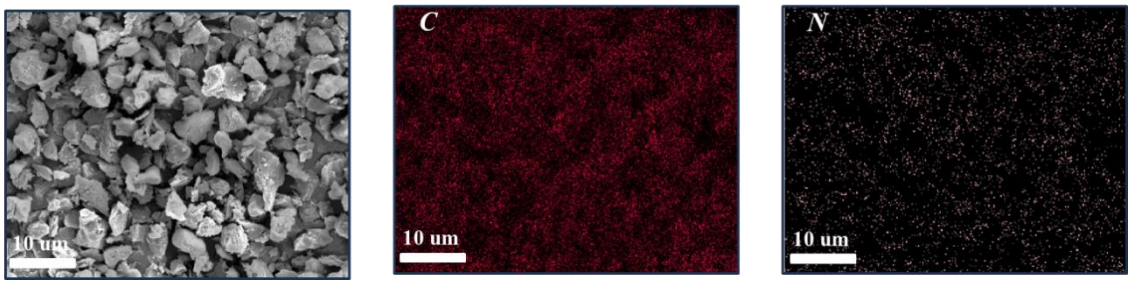

Fig. S4 SEM image of NKCOF41 and elemental (C and N) mapping images.

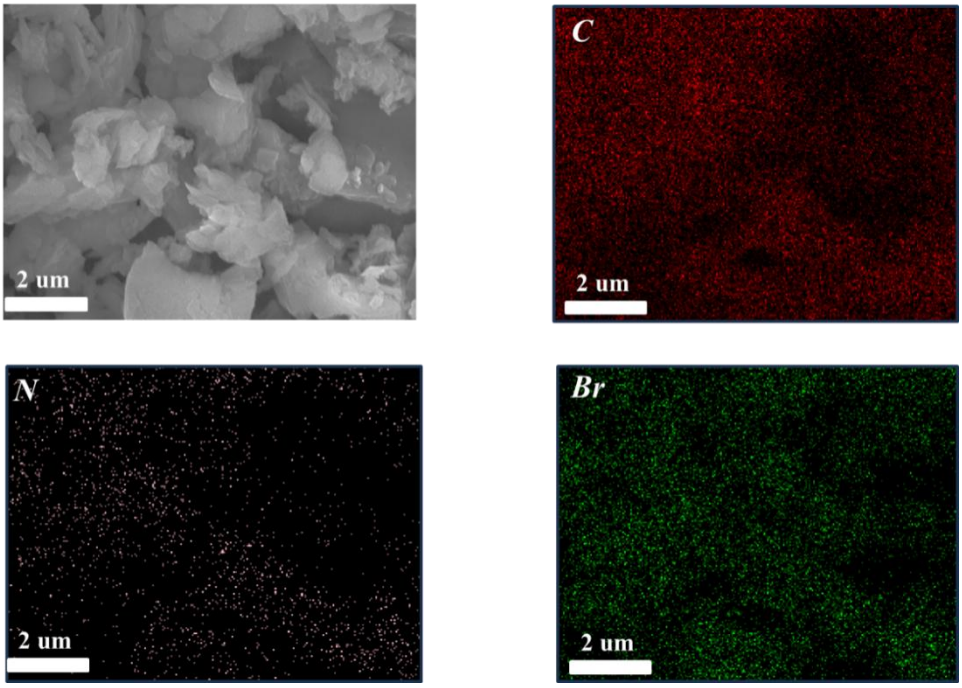

Fig. S5 SEM image of NKCOF41H^+–Br^- and elemental (C, N, and Br) mapping images.

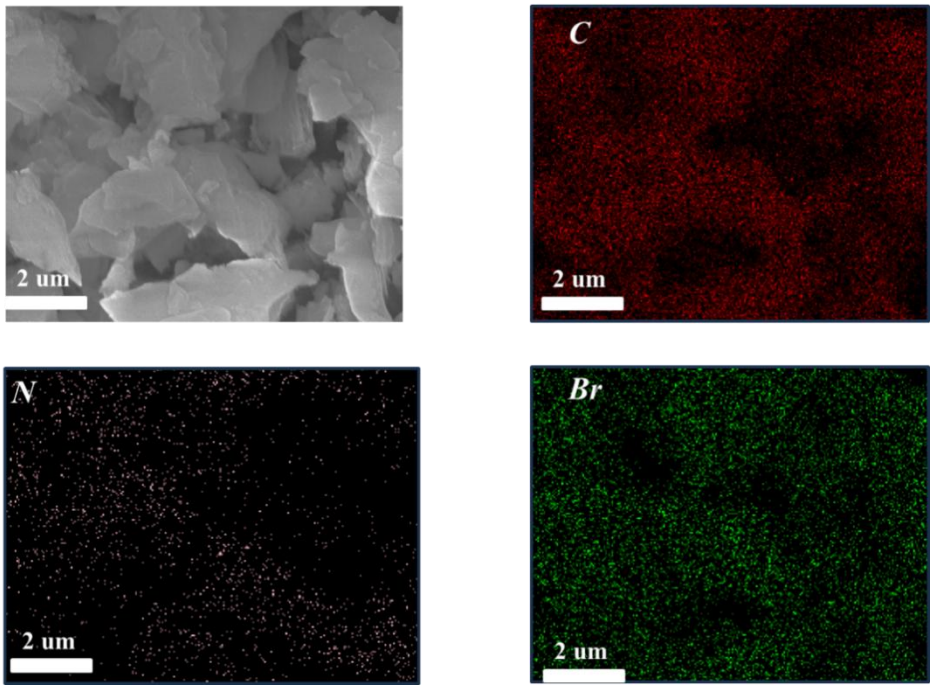

Fig. S6 SEM image of NKCOF41$^+$–$C_2H_5Br^-$ and elemental (C, N, and Br) mapping images

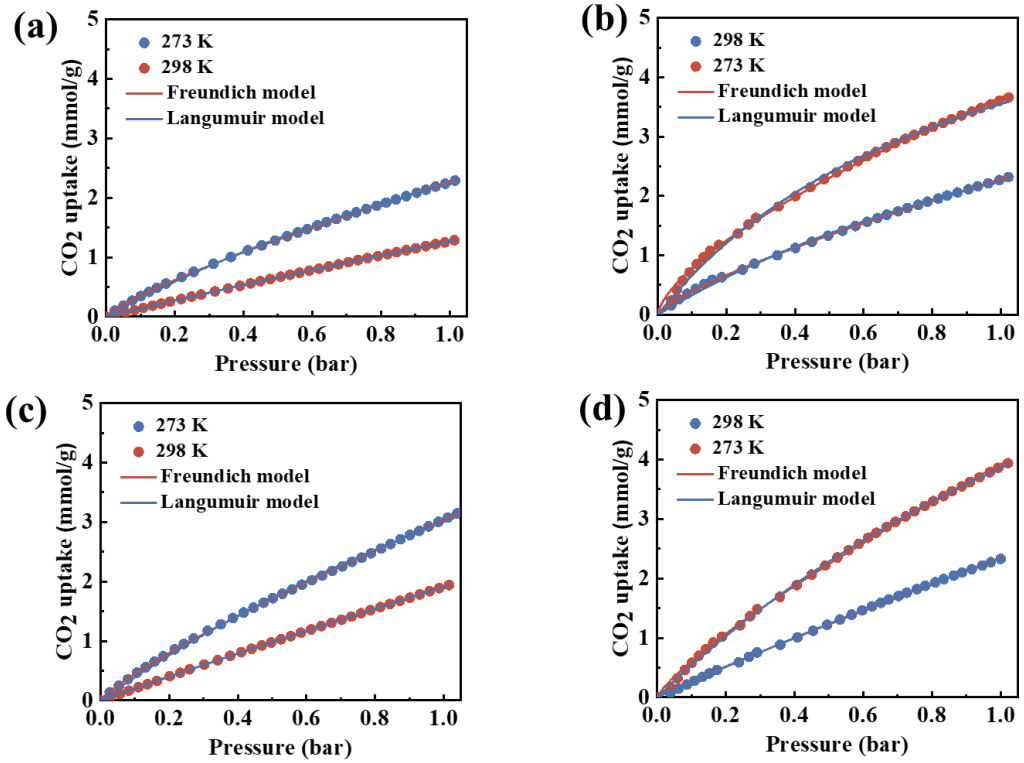

Fig. S7 Non-linear curve fitting of CO_2 adsorption isotherms (273 and 298 K) of NKCOF41, NKCOF41H^+–Br^-, NKCOF41$^+$–$C_2H_5Br^-$, and NKCOF41$^+$–$C_2H_4OHBr^-$.

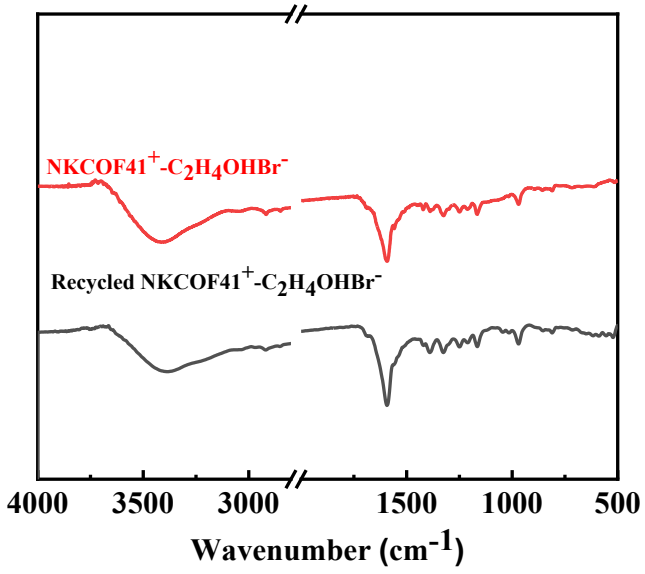

Fig. S8. FT-IR spectra of fresh and recycled NKCOF41$^+$–$C_2H_4OHBr^-$.

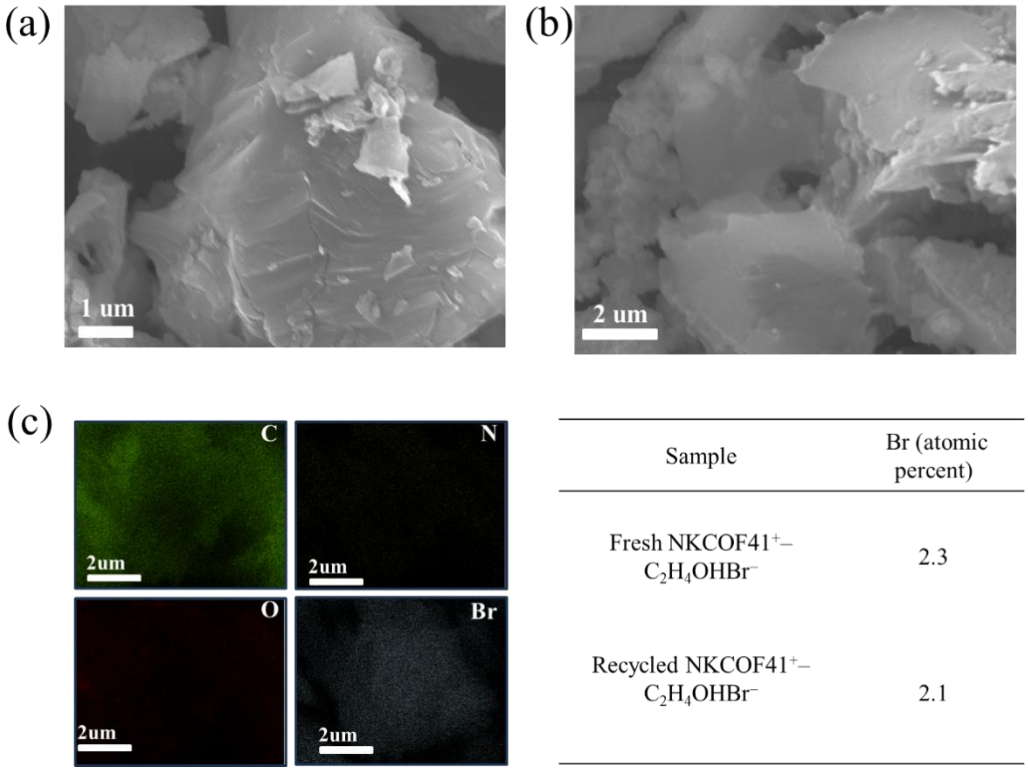

Sample	Br (atomic percent)
Fresh NKCOF41^{+}–$C_2H_4OHBr^{-}$	2.3
Recycled NKCOF41^{+}–$C_2H_4OHBr^{-}$	2.1

Fig. S9. (a, b) SEM images of fresh and recycled NKCOF41^{+}–$C_2H_4OHBr^{-}$, (c) EDS image of recycled NKCOF41^{+}–$C_2H_5Br^{-}$.

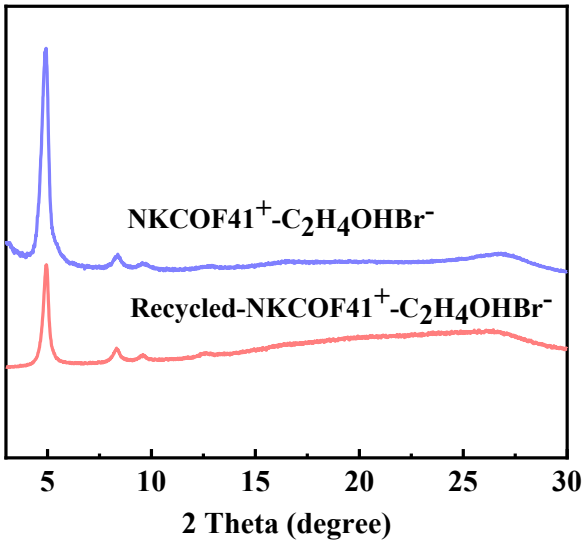

Fig. S10. XRD images of fresh and recycled NKCOF41^{+}–$C_2H_4OHBr^{-}$.

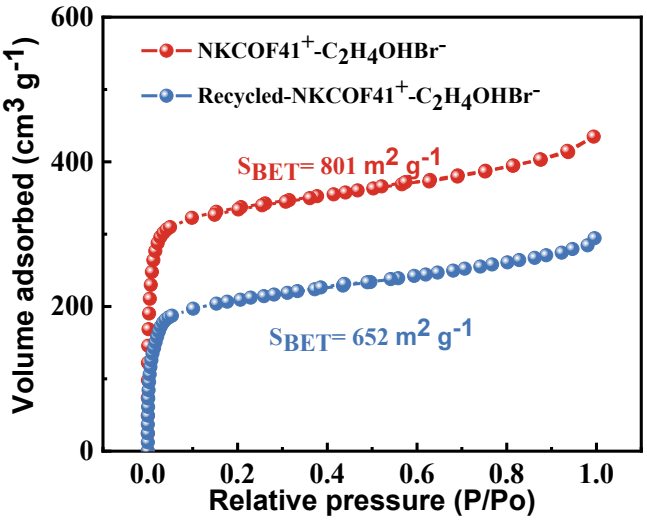

Fig. S11. N_2 adsorption-desorption isotherms of fresh and recycled NKCOF41^{+}–$C_2H_4OHBr^{-}$.

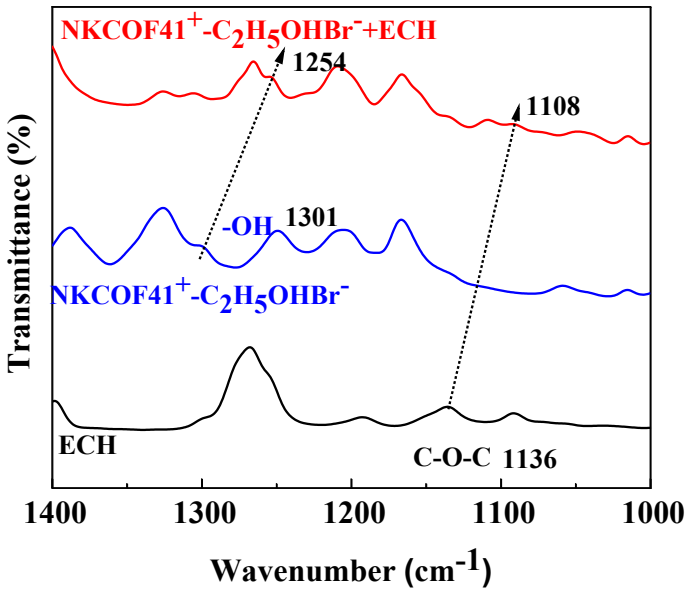

Fig. S12 FT-IR spectra of ECH, ECH + NKCOF41^{+}–$C_2H_4OHBr^{-}$, and NKCOF41^{+}–$C_2H_4OHBr^{-}$

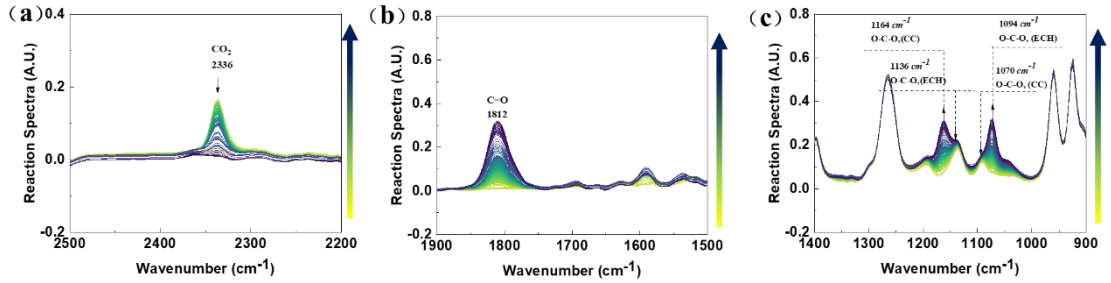

Fig. S13 In-situ react IR spectra of NKCOF41^{+}–$C_2H_4OHBr^{-}$ catalyzing CO_2-ECH cycloaddition at ambient pressure and 60 °C for 12 h

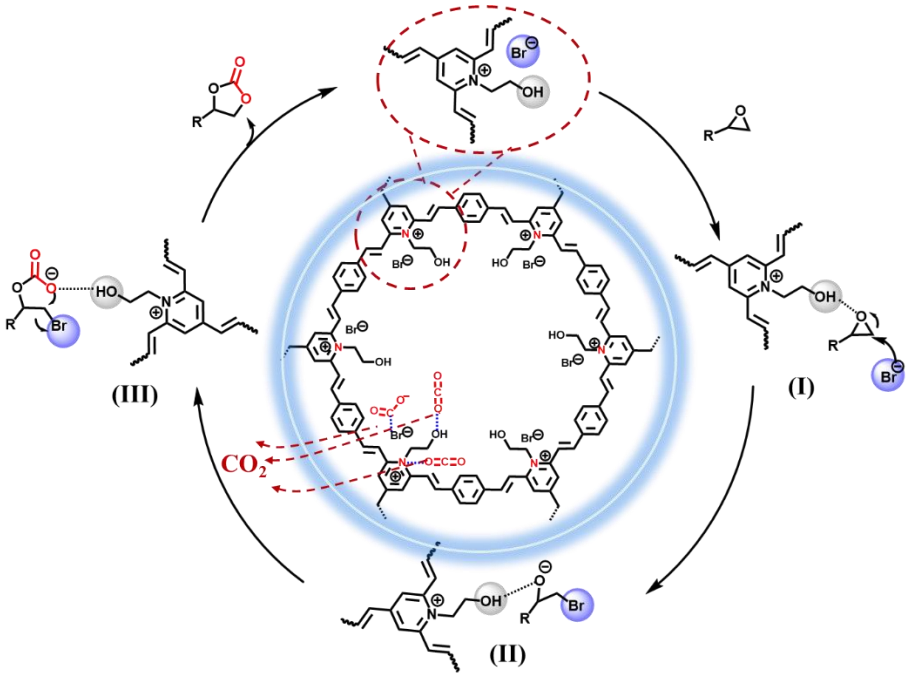

Fig. S14 Illustration of the proposed mechanism for the cycloaddition reaction between CO_2 and epoxide catalyzed by the NKCOF41^{+}–$C_2H_4OHBr^{-}$.

Table S1. Summary of specific surface area, pore size, and CO_2 adsorption of COFs.

COF	S_{BET} ($m^2\ g^{-1}$)	V_{Total} ($cm^3\ g^{-1}$)	Pore size (nm)	CO_2 uptake (mmol g^{-1})	
				273 K	298 K
NKCOF41	1337	0.774	1.41	2.29	1.29
NKCOF41^{+}–$C_2H_5Br^{-}$	875	0.642	1.13	3.15	1.94
NKCOF41H^{+}–Br^{-}	980	0.673	1.13	3.66	2.32
NKCOF41^{+}–$C_2H_4OHBr^{-}$	801	0.538	1.13	3.94	2.33

Table S2. Corresponding parameters after fitting Langmuir and Freundich.

COF	T(K)	Q_{exp}	Langumuir				Freundich			
			q_{mod}	Q_{max}	kl	R^2	q_{mod}	K_f	n	R^2
NKCOF41	273.15	2.290	2.256	7.3735	0.434	0.998	2.293	1.273	1.241	0.999
	298.15	1.287	1.284	15.5387	0.089	0.999	2.290	2.265	1.050	0.999
NKCOF41H^+–Br^-	273.15	3.659	3.588	6.9311	1.049	0.997	3.713	3.656	1.496	0.998
	298.15	2.316	2.275	6.326	0.550	0.997	2.316	2.281	1.301	0.999
NKCOF41$^+$–$C_2H_5Br^-$	273.15	3.147	3.090	11.479	0.354	0.998	1.942	3.032	1.207	0.999
	298.15	1.940	1.937	35.488	0.057	0.999	3.132	1.913	1.033	0.999
NKCOF41$^+$–$C_2H_4OHBr^-$	273.15	3.938	3.913	12.413	0.451	0.999	3.990	3.923	1.237	0.999
	298.15	2.330	2.337	21.228	0.124	0.999	2.354	2.354	1.065	0.999

Table S3. Comparison of the CO_2 capture capacity of different COFs and ionic materials.

Entry	Material	S_{BET} (m^2 g^{-1})	CO_2 uptake (mmol g^{-1})		Ref.
			273 K	298 K	
1	PPIL@COFA-40	752	1.28		[1]
2	COF─CN	486	1.43		[2]
3	HPMBr0.5	558	1.74	0.93	[3]
4	Fe^{3+}doped Py-1P COFs	1718	1.8	1.21	[4]
5	[HBIM-2]Br^-BCB (1)	440	2.02	1.36	[5]
6	PyTTA-BFBIm-ionic COFs	1532	2.11		[6]
7	Meso-PR-36	782	2.16	1.32	[7]
8	TAPT-BP^{2+}-COF	473.5	2.54	1.52	[8]
9	TFPA-TAPA	1091	2.56		[9]
10	Gua-HCPIP-4	598	2.72		[10]
11	PTPIM	542	2.77	1.72	[11]
12	NHC-CAP-1(Zn^{2+})	1040	2.80	1.72	[12]
13	3D-BMTA-COF-[Ac]50%	1140	3.17	1.72	[13]
14	[Et_4NBr]50%-PyCOF	879	3.75	1.97	[14]
15	[HO_2C]100%-H_2P-COF	364	3.95		[15]
16	NKCOF41$^+$-$C_2H_4OHBr^-$	801	3.94	2.33	This work

3.NMR spectra of the cyclic carbonate products

4-phenyl-1,3-dioxolan-2-one: ^{1}H NMR (400 MHz, Chloroform-*d*) δ 7.34 (dt, *J* = 6.1, 2.5 Hz, 3H), 7.27 (dd, *J* = 7.4, 2.3 Hz, 2H), 5.59 (t, *J* = 8.0 Hz, 1H), 4.71 (t, *J* = 8.4 Hz, 1H), 4.25 (dd, *J* = 8.6, 7.9 Hz, 1H). ^{13}C NMR (101 MHz, Chloroform-*d*) δ 155.27, 136.17, 130.06, 129.56, 126.27, 78.38, 71.54.

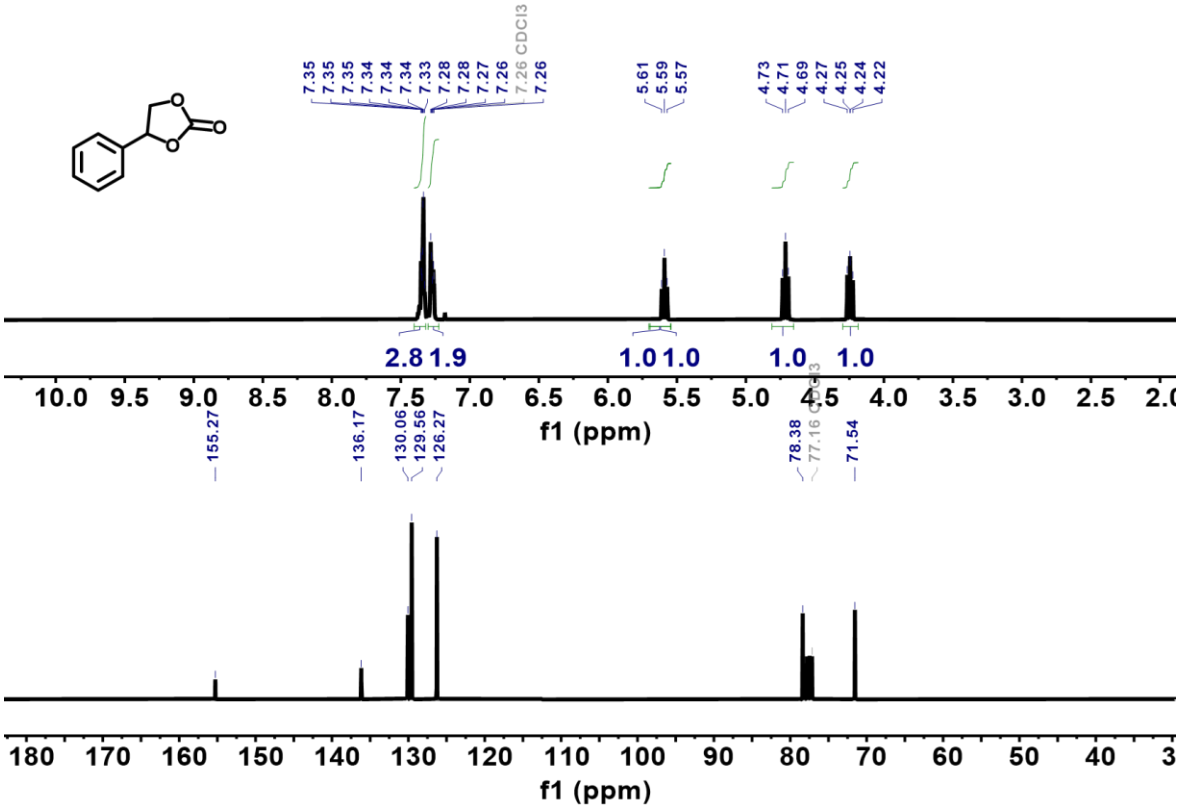

4-methyl-1,3-dioxolan-2-one: ^{1}H NMR (400 MHz, Chloroform-*d*) δ 4.80 (td, *J* = 7.4, 6.2 Hz, 1H), 4.49 (t, *J* = 8.1 Hz, 1H), 3.95 (dd, *J* = 8.5, 7.2 Hz, 1H), 1.40 (d, *J* = 6.3 Hz, 3H). ^{13}C NMR (101 MHz, Chloroform-*d*) δ 155.41, 73.95, 70.95, 19.50.

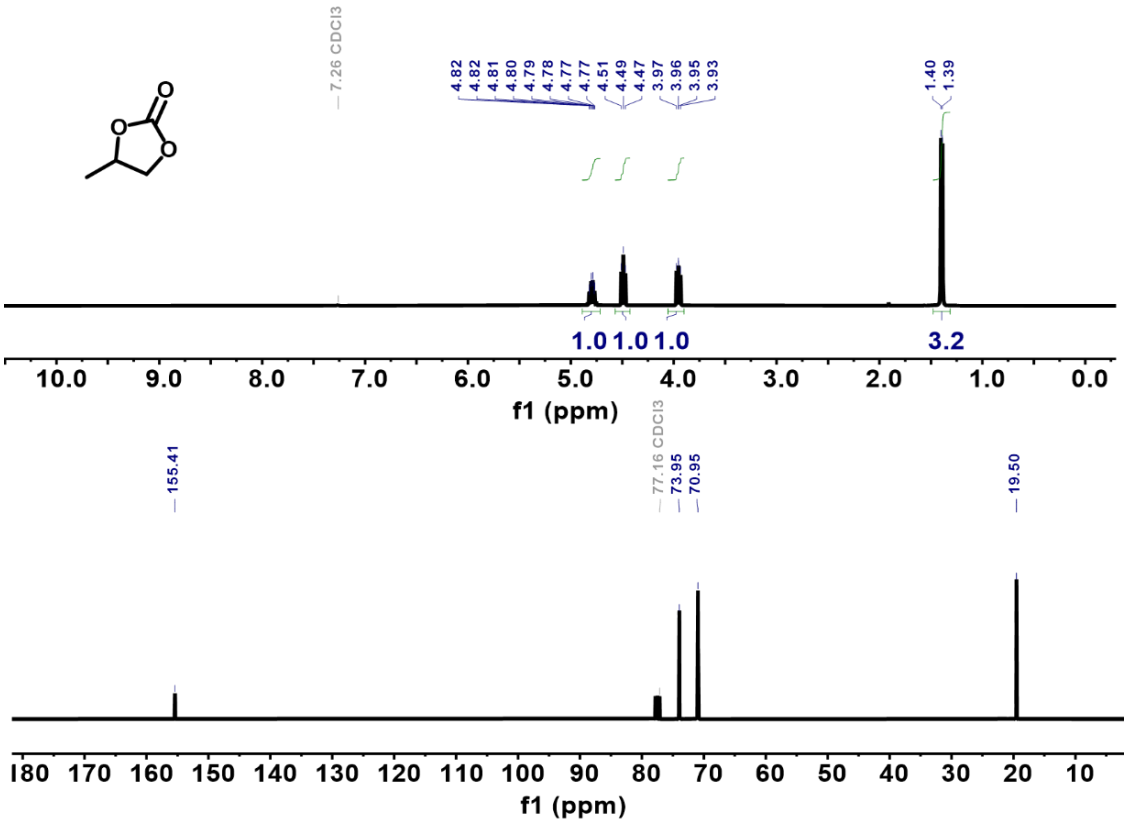

4-(chloromethyl)-1,3-dioxolan-2-one:[1]H NMR (400 MHz, Chloroform-*d*) δ 4.98 (dddd, *J* = 8.3, 5.7, 4.5, 3.6 Hz, 1H), 4.55 (t, *J* = 8.6 Hz, 1H), 4.34 (dd, *J* = 8.9, 5.7 Hz, 1H), 3.88 – 3.64 (m, 2H). [13]C NMR (101 MHz, Chloroform-*d*) δ 154.85, 74.80, 67.21, 44.48

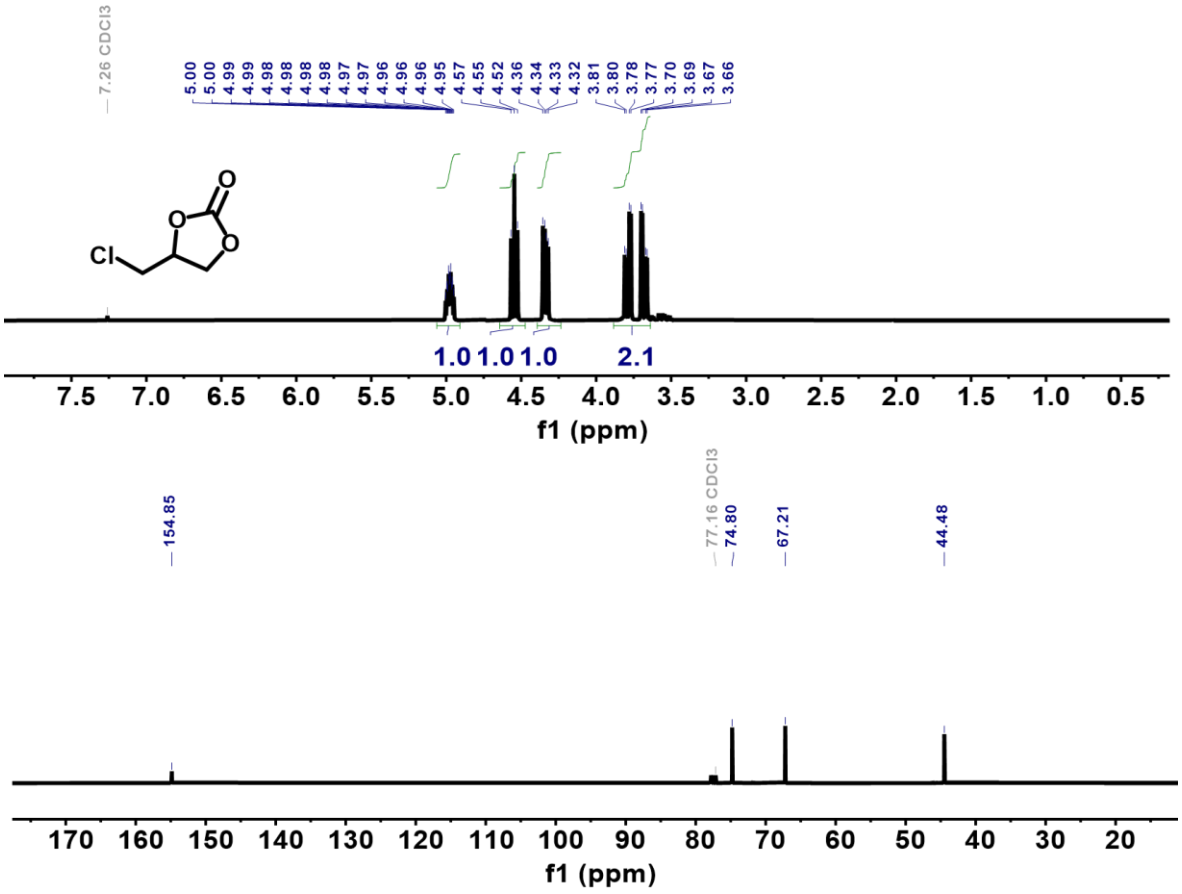

4-(bromomethyl)-1,3-dioxolan-2-one:[1]H NMR (400 MHz, Chloroform-*d*) δ 4.96 (ddd, *J* = 10.7, 8.1, 5.3 Hz, 1H), 4.69 – 4.55 (m, 1H), 4.36 (dd, *J* = 8.7, 5.9 Hz, 1H), 3.58 (d, *J* = 5.0 Hz, 2H). [13]C NMR (101 MHz, Chloroform-*d*) δ 154.35, 74.08, 68.26, 31.55.

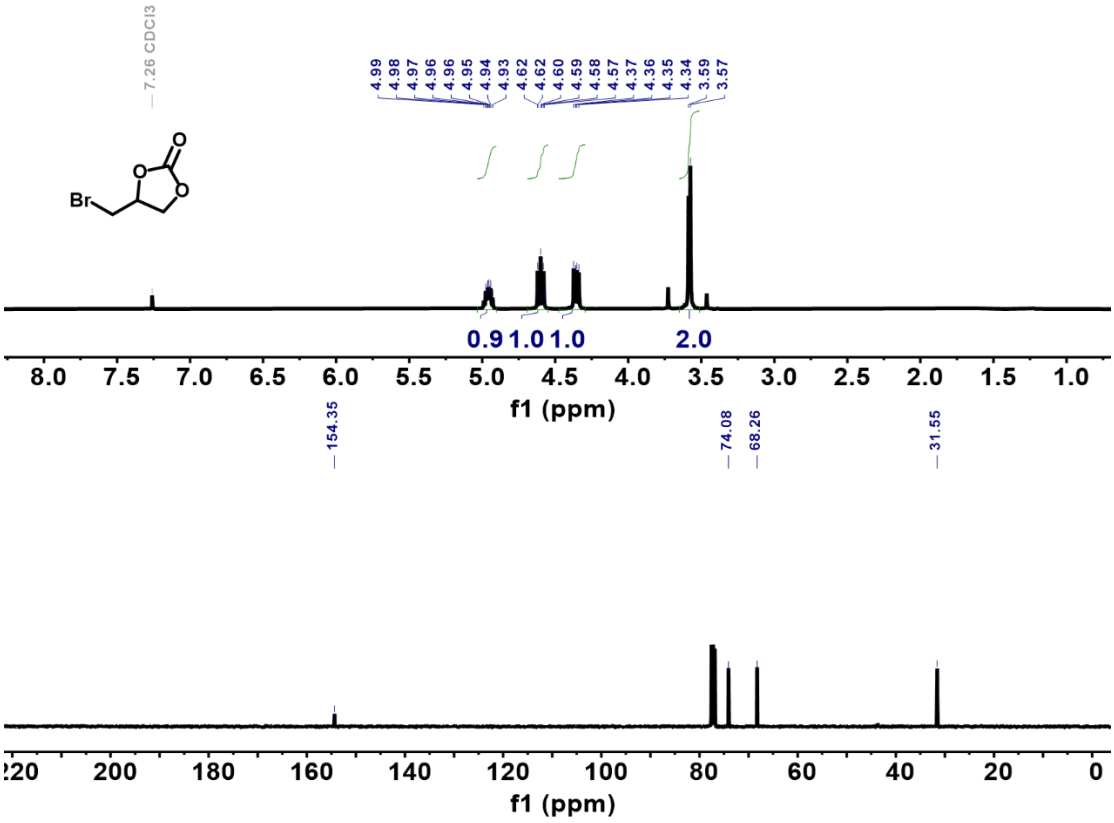

4-(pent-4-en-1-yl)-1,3-dioxolan-2-one (4a): ^{1}H NMR (400 MHz, Chloroform-*d*) δ 4.72 (ddt, *J* = 9.1, 6.3, 3.4 Hz, 1H), 4.39 (t, *J* = 8.4 Hz, 1H), 4.24 (dd, *J* = 8.4, 5.9 Hz, 1H), 3.56 (dd, *J* = 11.2, 3.2 Hz, 1H), 3.46 (dd, *J* = 11.3, 3.6 Hz, 1H), 3.38 (dd, *J* = 6.9, 5.9 Hz, 2H), 1.42 (dq, *J* = 8.4, 6.6 Hz, 2H), 1.33 – 1.16 (m, 2H), 0.78 (t, *J* = 7.4 Hz, 3H). ^{13}C NMR (101 MHz, Chloroform-*d*) δ 154.75, 74.95, 71.08, 69.07, 65.72, 30.93, 18.54, 13.22.

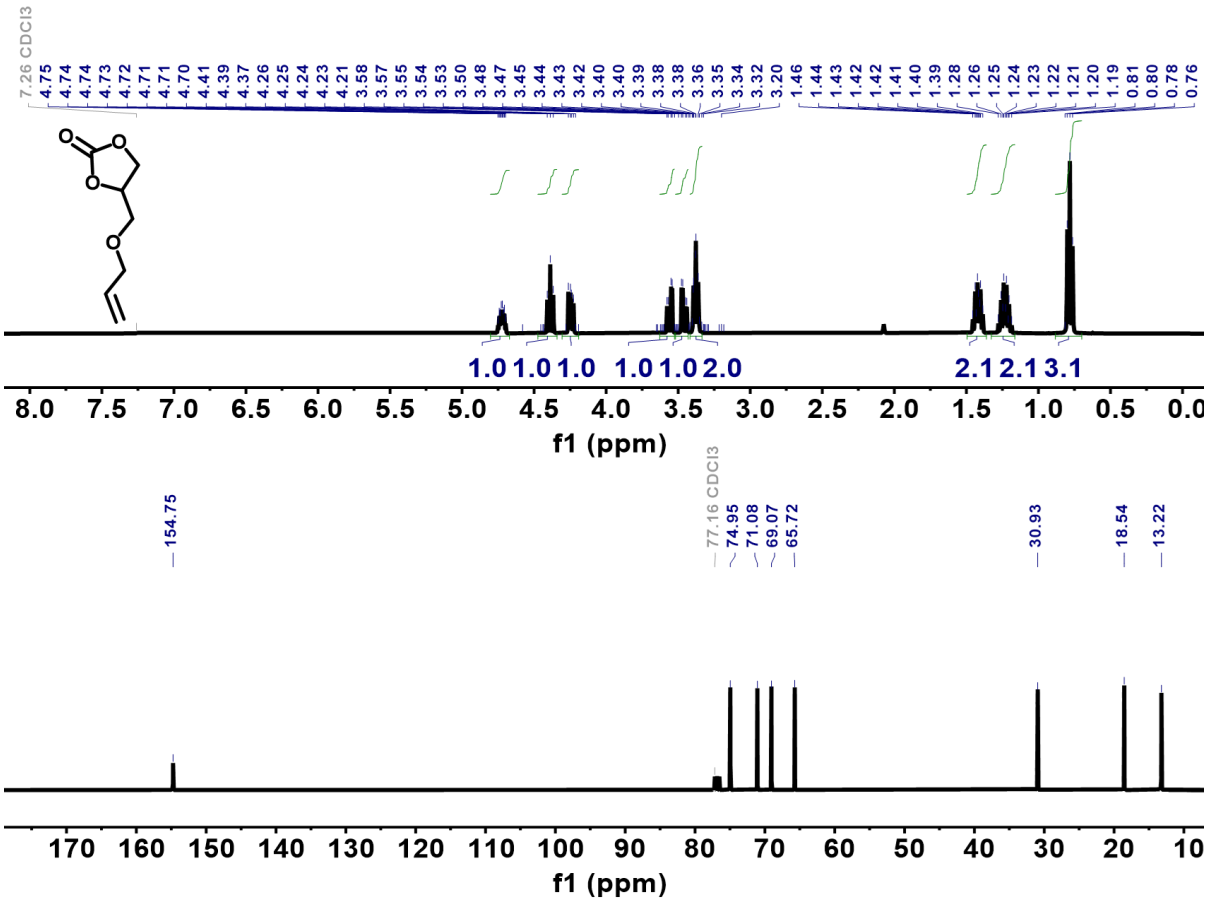

4-(butoxymethyl)-1,3-dioxolan-2-one: ^{1}H NMR (400 MHz,) δ 5.86 (ddd, *J* = 22.6, 10.8, 5.7 Hz, 1H), 5.39 – 5.12 (m, 2H), 4.83 (ddt, *J* = 7.9, 5.8, 3.8 Hz, 1H), 4.50 (t, *J* = 8.3 Hz, 1H), 4.40 (dd, *J* = 8.5, 6.0 Hz, 1H), 4.13 – 3.97 (m, 2H), 3.69 (dd, *J* = 11.0, 3.8 Hz, 1H), 3.61 (dd, *J* = 11.0, 3.8 Hz, 1H). ^{13}C NMR (101 MHz, Chloroform-*d*) δ 154.80, 133.40, 117.83, 74.80, 72.37, 68.55, 66.06.

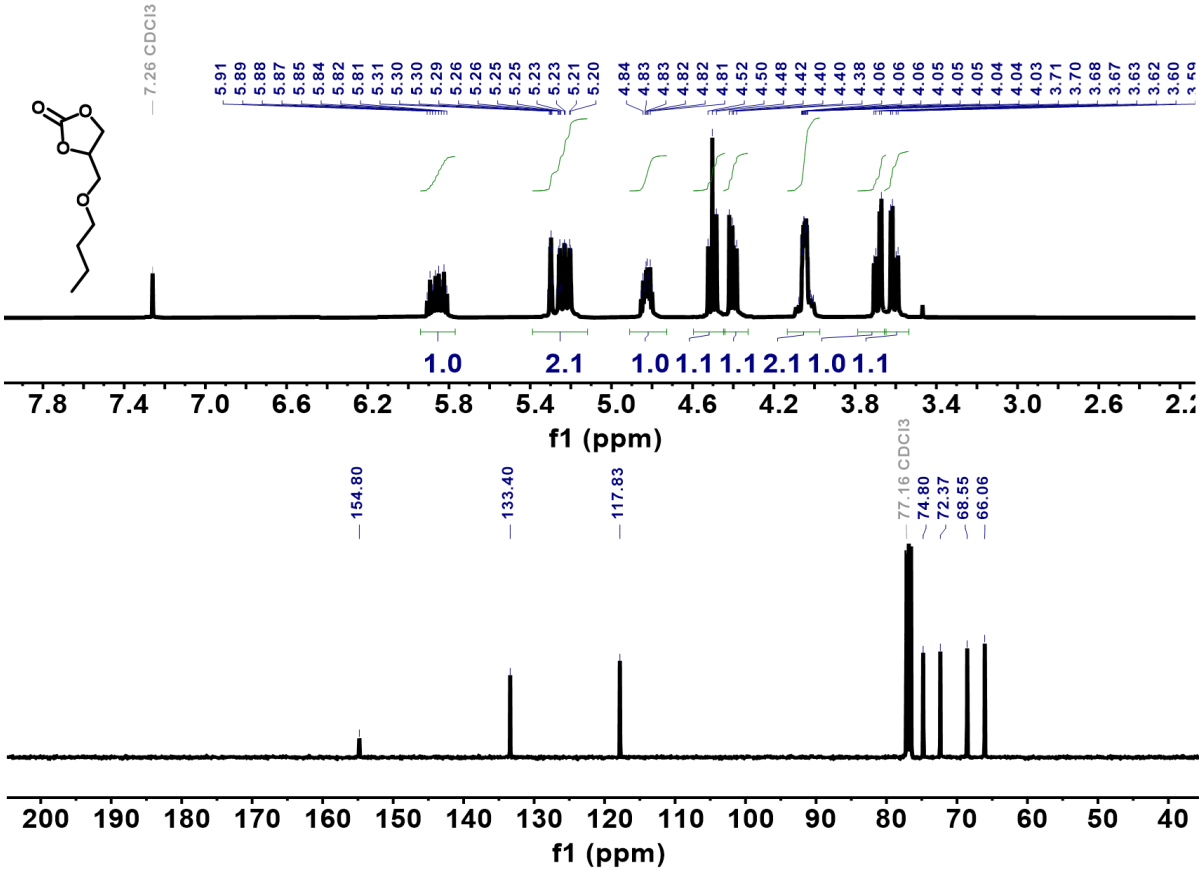

4-butyl-1,3-dioxolan-2-one:[1]H NMR (400 MHz, Chloroform-*d*) δ 4.77 – 4.62 (m, 1H), 4.52 (t, *J* = 8.2 Hz, 1H), 4.13 – 3.99 (m, 1H), 1.77 (ddd, *J* = 13.6, 7.8, 4.8 Hz, 1H), 1.67 (ddd, *J* = 14.1, 9.7, 5.0 Hz, 1H), 1.50 – 1.24 (m, 4H), 0.90 (t, *J* = 7.0 Hz, 3H). [13]C NMR (101 MHz, Chloroform-*d*) δ 155.30, 69.51, 33.60, 26.48, 22.31, 13.90.

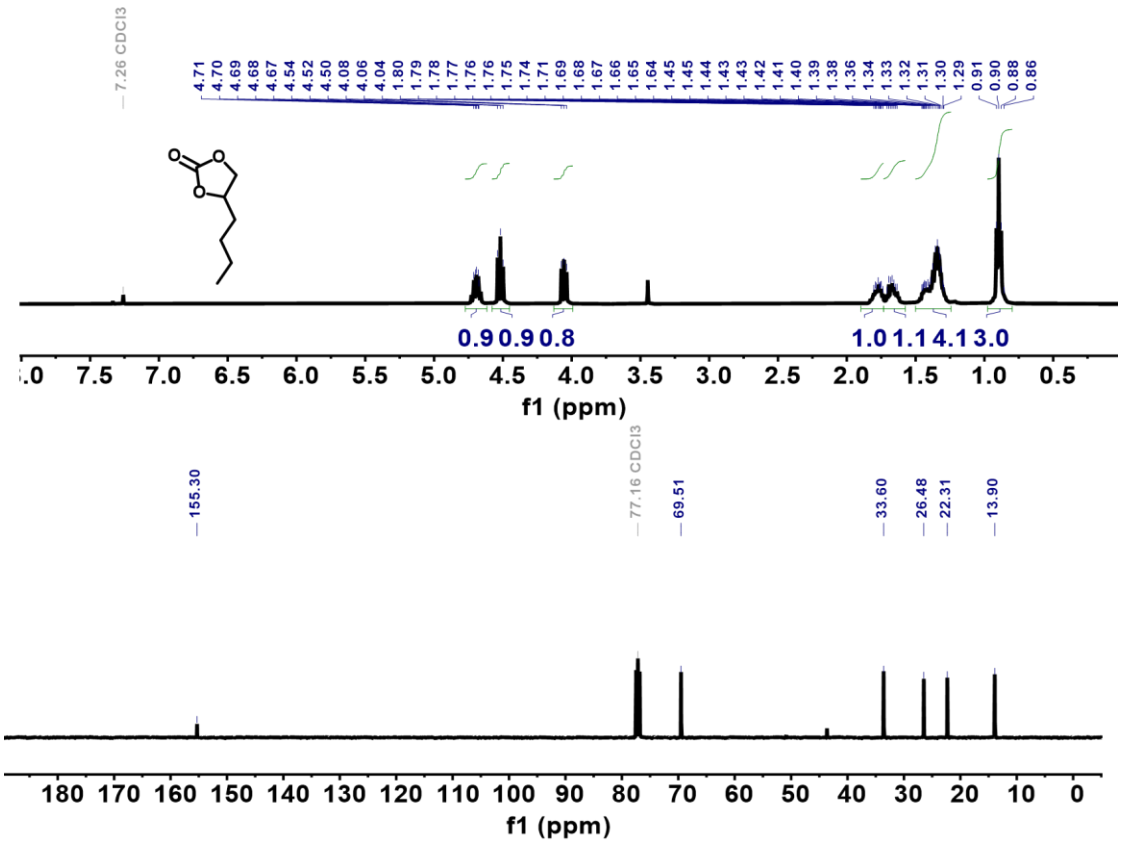

4-(phenoxymethyl)-1,3-dioxolan-2-one: ^{1}H NMR (400 MHz, DMSO-d_6) δ 7.31 (td, J = 8.0, 7.5, 4.9 Hz, 2H), 6.97 (dt, J = 8.2, 3.7 Hz, 3H), 5.15 (dqd, J = 8.3, 5.2, 2.5 Hz, 1H), 4.63 (td, J = 8.4, 4.8 Hz, 1H), 4.39 (dt, J = 8.5, 5.2 Hz, 1H), 4.28 (dq, J = 11.4, 2.7 Hz, 1H), 4.24 – 4.17 (m, 1H). ^{13}C NMR (101 MHz, DMSO-d_6) δ 157.73, 154.65, 129.40, 121.04, 114.40, 74.62, 67.18, 65.82.

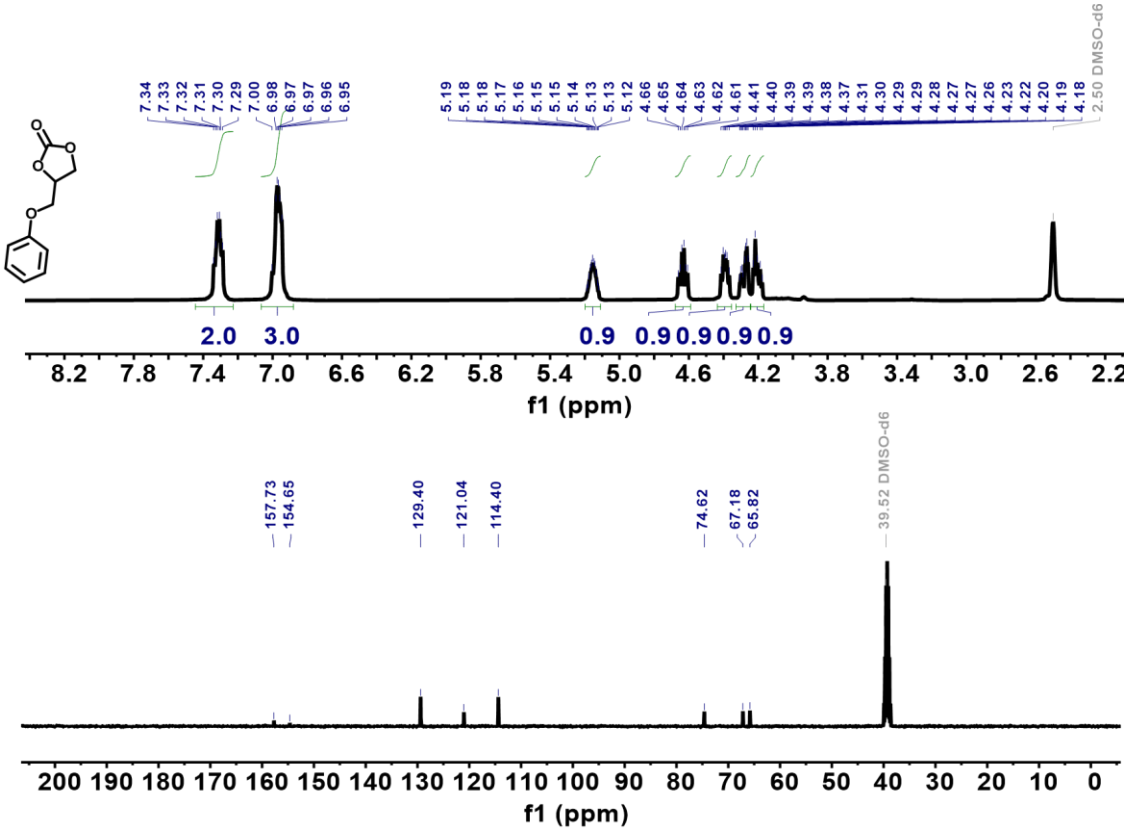

3. References

1 Y.-R. Du, G.-R. Ding, Y.-F. Wang, B.-H. Xu and S.-J. Zhang, *Green Chem.*, 2021, **23**, 2411-2419..

2 X. Gu, H. Niu, H. Ding, W. Zhang, Y. Shi and Y. Cai, *Adv. Funct. Mater.*, 2025, **35**, 2422116.

3 H. Lyu, X. Wang, W. Sun, E. Xu, Y. She, A. Liu, D. Gao, M. Hu, J. Guo, K. Hu, J. Cheng, Z. Long, Y. Liu and P. Zhang, *Green Chem.*, 2023, **25**, 3592-3605.

4 C. Kang, Z. Zhang, S. Xi, H. Li, A. K. Usadi, D. C. Calabro, L. S. Baugh, Y. Wang and D. Zhao, *P Natl Acad. Sci.*, 2023, **120**, e2217081120.

5 X. Liao, Z. Wang, Z. Li, L. Kong, W. Tang, Z. Qin and J. Lin, *Chem. Eng. J.* 2023, **471**, 144455.

6 N. Huang, X. Chen, R. Krishna and D. Jiang, *Angew. Chem. Int. Ed.*, 2015, **54**, 2986-2990.

7 J. Zhang, Z.-A. Qiao, S. M. Mahurin, X. Jiang, S.-H. Chai, H. Lu, K. Nelson and S. Dai, *Angew. Chem. Int. Ed.*, 2015, **54**, 4582-4586.

8 M. Yin, L. Wang and S. Tang, *ACS Catal.* 2023, **13**, 13021-13033.

9 A. Dey, D. Brahma, S. Laha, V. R. Bakuru, S. R. V. Parambil, A. Singh, S. Balasubramanian and T. K. Maji, *Chem. Mater.*, 2025, **37**, 4314-4324

10 X. Yang, J. Zhao, J. Zeng, B. Chen, L. Tang, J. Zhang, A. Zeb, Z. Li, S. Zhang and Y. Zhang, *Green Chem.*, 2025, **27**, 1729-1739

11 G. Feng, M. Yang, H. Chen, B. Liu, Y. Liu and H. Li, *Sep. Purifi. Technol.*, 2023, **323**, 124484

12 P. Puthiaraj, S. Ravi, K. Yu and W.-S. Ahn, *Applied Catalysis B: Environmental*, 2019, **251**, 195-205.

13 B. Gui, X. Liu, Y. Cheng, Y. Zhang, P. Chen, M. He, J. Sun and C. Wang, *Angew. Chem. Int. Ed.*, 2022, **61**, e202113852.

14 B. Dong, L. Wang, S. Zhao, R. Ge, X. Song, Y. Wang and Y. Gao, *Chem. Commun.* 2016, **52**, 7082-7085.

15 N. Huang, P. Wang, M. A. Addicoat, T. Heine and D. Jiang, Angew. Chem. Int. Ed., 2017, **56**, 4982-4986.